Influence of Intermolecular Hydrogen Bonding on the Photochromic Cycle of the Aromatic Schiff Base *N*,*N*′-Bis(salicylidene)-*p*-phenylenediamine in Solution

Marcin Ziółek,*,†,‡ Gotard Burdziński,‡ and Jerzy Karolczak†,‡

Center for Ultrafast Laser Spectroscopy, and Quantum Electronics Laboratory, Faculty of Physics, Adam Mickiewicz University, Umultowska 85, 61-614 Poznan, Poland

Received: May 1, 2008; Revised Manuscript Received: January 14, 2009

A photochromic symmetric Schiff base, *N*,*N*′-bis(salicylidene)-*p*-phenylenediamine, has been studied by means of stationary and time-resolved spectroscopic absorption and emission techniques in the UV−vis spectral range with particular attention to the role of intermolecular hydrogen bonds. They are found to be responsible for the solvent-assisted excited-state proton transfer (the time constant of about 400 fs) in very strongly protic solvents and the photochrome deactivation (the time constant from 0.5 μs to 3 ms) in both protic and nonprotic solvents. Moreover, formation of an isomer that competes with the photochromic cycle in solution is also observed.

Introduction

N,*N*′-Bis(salicylidene)-*p*-phenylenediamine (BSP) is a symmetric aromatic Schiff base belonging to the family of salicylideneaniline (SA) (see Scheme 1). The photochromism of the molecules from this family attracts much interest because of possible applications, e.g., in molecular memories and switches.[1] SA and its derivatives are characterized by a very good fatigue factor,[2] and the lifetime of its photochromic form in the crystal state can be as long as several hundred days.[3] The primary and photochromic forms differ significantly in nonlinear optical properties, which can be employed in optical logic devices based on generation of higher harmonics.[3] The simplest and commonly assumed photochromic cycle of SA family is the following.[4,5] After the excitation of the initial enol (anti-enol) tautomer, the ultrafast excited-state intramolecular proton transfer (ESIPT) takes place, leading to the excited keto tautomer (cis-keto or its zwitterionic form), exhibiting a characteristic, strongly Stokes shifted fluorescence band. Then, after the structural changes (rotation around C=C and/or C−N bond; see Scheme 1) involving the cleavage of the intramolecular hydrogen bond, the long-lived photochromic tautomer (trans-keto or its zwitterionic form) in the ground state is generated. The lifetime of the latter is on the order of microseconds and milliseconds at room temperature[4,5] but can increase up to minutes and hours at lower temperatures.[6,7]

BSP molecule has been initially studied in the solid state, in which it shows its thermochromic properties.[8,9] On the contrary, BSP in solution exhibits photochromic behavior, and the spectroscopic properties of cis-keto and trans-keto forms are very similar to those of SA.[4,5] Therefore, it has been concluded that, despite the two possible proton transfer centers, the excitation of BSP in solution is localized on one salicylidene subunit. Consequently, it is the site of the proton transfer reactivity, and BSP upon excitation undergoes the single proton transfer, leading to the excited monoketo tautomer (therefore, for simplicity, this tautomer will be called "keto" throughout this paper). Because of its symmetry, BSP has been also recently studied in the aspects of fluorescent nanoparticles[10] and multicomponent material design.[11] Theoretical calculations predict the additivity of the photochemical properties of the two subunits: the change in one subunit does not alter significantly the features of the other.[11]

SCHEME 1: Different Tautomers of the BSP Molecule[a] and the Formulae of $BSPMe_2$ and the Parent SA Molecule

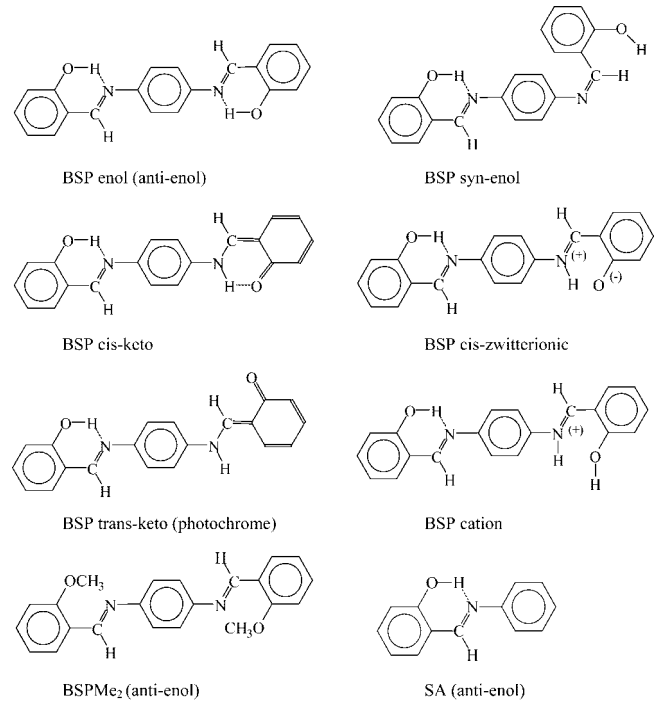

[a] For simplicity all structures are presented as planar ones.

Recently, we have studied BSP by means of stationary and time-resolved (on femto- and picosecond time scale) absorption and emission methods in nonpolar, polar, and protic solvents.[12,13] One of the facts that inspired this study was that the signal of transient absorption of BSP from the excited enol form shows a prominent band in the spectral range overlapping the negative

* Corresponding author. Tel: (48) 61-829-5011. E-mail: marziol@amu.edu.pl.
† Center for Ultrafast Laser Spectroscopy.
‡ Quantum Electronics Laboratory.

10.1021/jp803850n CCC: $40.75
Published on Web 02/25/2009

signal of the stimulated emission of the keto form. This would enable a clear observation of the very fast dynamics of the ESIPT reaction in BSP unlike in other molecules from the SA family.[14] Moreover, BSP is particularly suitable for the measurements on the ultrafast time scale, because the spectral position of its absorption band fits the second harmonic (about 400 nm) of commonly available Ti:sapphire lasers. The most important findings are the following.[13] After the excitation of the enol form to the excited singlet state $S_1(\pi,\pi^*)$, the latter deactivates within 50 fs by two ultrafast processes of comparable rate constants: ESIPT reaction, leading to the $S_1(\pi,\pi^*)$ state of keto tautomer, and electronic relaxation to the $S_1(n,\pi^*)$ enol state. The same fluorescent $S_1(\pi,\pi^*)$ state of keto tautomer is formed after the direct excitation of its ground state (in protic solvents) and via ESIPT reaction. The intermolecular hydrogen bonds are present in solvents of hydrogen-bond-donation ability up to that of trifluoroethanol, but they do not break up the strong intramolecular hydrogen bond and do not influence the ESIPT dynamics.

The key role of the intramolecular hydrogen bonding in the photochromic cycle of Schiff bases is obvious, since ESIPT is the starting point of the cycle. However, the role of the intermolecular hydrogen bonds has not been well examined, despite its importance in the photochromism of these compounds in solution. Therefore, the aim of the present paper is to extend the previous studies of BSP with particular interest in the influence of the intermolecular hydrogen bonding. First, the spectroscopic investigation (similar to previous one) in even more protic solvents than trifluoroethanol is employed. Second, the properties of photochromic transient of BSP are studied on nano- and microsecond time scale in different solvents including strongly protic ones. The studies for BSP should be also relevant for a large group of aromatic Schiff bases (at least those belonging to the SA family).

Experimental Section

BSP was synthesized by conventional condensation of *p*-phenylenediamine and salicylaldehyde. The sample was additionally recrystallized from $CHCl_3$. All measurements were performed at room temperature. The following solvents were used: acetonitrile (ACN, for fluorescence, Merck), hexane (HEX, for HPLC, Merck), ethanol (EtOH, 99.8%, POCh), methanol (MeOH, for HPLC, Merck), trifluoroethanol (TFE, 99.5%, Aldrich), hexafluoroisopropyl alcohol (HFIP, 99%, Aldrich), and trifluoroacetic acid (TFA, for spectroscopy, Merck). The concentration of BSP was about 3×10^{-5} M.

The equipment for stationary measurements was the same as described in our previous papers.[13,15] Briefly, the stationary UV−vis absorption spectra were measured with a UV−vis-550 (Jasco) spectrophotometer. The steady-state fluorescence emission spectra were recorded with a FL900 spectrofluorimeter (Edinburgh Instruments) with a laser as an excitation source or with a modified SPF-500 (Aminco-Bowman) spectrofluorimeter (with the single-photon counting detection). The latter spectrofluorimeter was also used to measure the fluorescence quantum yields (ϕ_F), using quinine sulfate in 0.1 N sulfuric acid as the standard ($\phi_F = 0.53$). All fluorescence spectra were corrected for the wavelength sensitivity of the detection system.

The apparatus used for the time-resolved emission measurements (time-correlated single-photon counting, TCSPC) and for the transient absorption measurements was described in detail earlier.[16,17] The repetition rate of the laser system for the time-resolved emission measurements (Ti:sapphire) was set at 4 MHz, providing pulses of about 1 ps duration. The experiments were carried out at the magic angle, and the pump wavelength was 400 or 425 nm. The temporal resolution of the spectrofluorimeter was about 1 ps, and the spectral resolution was 9 nm.

The repetition rate of the laser system for the broad band transient absorption measurements (Ti:sapphire) was set at 1 kHz, providing pulses of about 100 fs duration. The probe beam was the white light continuum generated in a 2 mm rotating calcium fluoride plate. The thickness of the sample was 2 mm, the fwhm of the pump beam diameter at the sample was about 0.5 mm, the pump pulse energy was about 5 μJ, and the pump wavelengths was 400 nm. All the spectra analyzed were corrected for the chirp of the white light continuum. The pump−probe cross correlation function unaffected by the cell thickness was determined from the two-photon absorption in a very thin (150 μm) BK7 glass plate; its fwhm is 150 fs. The transient absorption signals, originating from the pure solvent, were subtracted from the data collected. The transient absorption measurements were performed in the spectral range of 330−730 nm and the temporal range of 0−200 ps. The transient absorption results of BSP in HFIP and in TFA were confirmed in three independent measurement sessions.

The nanosecond transient absorption setup used was also described earlier.[18] The pump pulse wavelength was 355 nm (Q-switched Nd:YAG laser) and the instrumental function was about 12 ns (fwhm). The probing light source was a 150 W xenon arc lamp. The transmitted light was dispersed by a monochromator and detected by a photomultiplier coupled to a digital oscilloscope. The spectral resolution was set at 10 nm and the pump pulse energy was about 1 mJ. The kinetics was recorded in the spectral range 300−750 nm every 12.5 or 25 nm. The temporal range was 10 ns−500 μs, determined by the duration of the laser pulse from one side and the lamp pulse from the other side.

Semiempirical calculations were performed with the PM6 method[19] under the MOPAC2007 package[20] According to the author of this method, the hydrogen bonds are represented more accurately in PM6 than in the other semiempirical methods.[19] Some ab initio calculation were also performed[21] (method MP2, basis set 6-31+G*). The calculations helped to find the optimized structures of different tautomers as well as their complexes with alcohol molecules (MeOH and HFIP). The stabilization energy of the complexes was calculated as the difference in their heat of formation with respect to the optimized structures of both molecules (BSP tautomer and alcohol) separately.

Results and Discussion

BSP Properties in a Strongly Protic Solvent. Previously, we have analyzed the spectroscopic properties of BSP in alcohols with hydrogen-bond-donation ability as large as TFE.[13] In this paper, we extend the studies to HFIP, which is a solvent of even greater proton-donating properties than TFE, and its acidlike behavior has been frequently reported. Thus, the time-resolved measurements of BSP in an acid (TFA) were also performed. Moreover, the dimethoxy derivative of BSP ($BSPMe_2$) (see Scheme 1), acting as a reference compound whose structure excludes the intramolecular hydrogen bond and proton transfer (the deactivation is exclusively connected within the enol type structure), was also investigated.

The stationary absorption as well as stationary and picosecond fluorescence studies do not indicate any additional features of BSP in HFIP compared to its behavior in weaker protic alcohols. The two absorption band maxima (see Figure 1) are at 349 and 435 nm and are blue-shifted with respect to those of TFE (358 and 440 nm) and those of EtOH and MeOH (369 nm and about

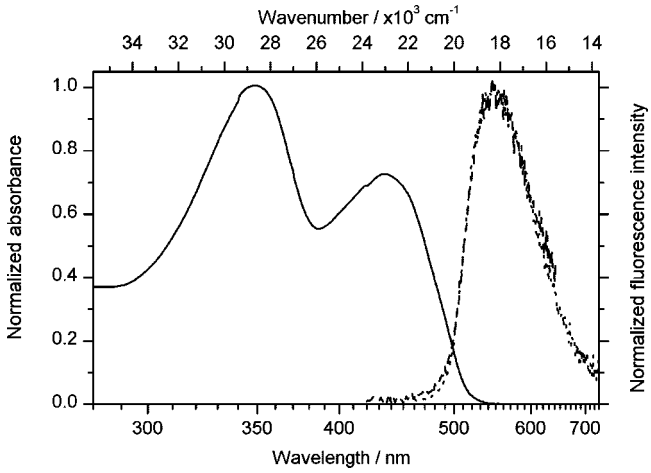

Figure 1. Stationary absorption spectra (solid line) and fluorescence spectra (dashed line, excitation at 360 nm; dotted line, excitation at 440 nm) of BSP in HFIP.

450 nm).[13] The short-wavelength band is due to the $S_1 \leftarrow S_0(\pi,\pi^*)$ transition of the enol tautomer, while the long-wavelength band occurring for many photochromic Schiff bases in protic solvents is usually ascribed to the $S_1 \leftarrow S_0(\pi,\pi^*)$ transition of proton-transferred cis-keto tautomer[7,13,22] (or its zwitterion form;[23] see Scheme 1). The interactions with strong protic solvents move the enol−keto equilibrium toward the cis-keto tautomer, since the ground state of the latter is more stabilized by hydrogen bonds with the solvent. For BSP in HFIP, the ratio of the cis-keto to enol absorbance is the highest ($A_K/A_E = 0.72$) and agrees well with the linear correlation between the $\log(A_K/A_E)$ and solvatochromic parameter describing the proton-donating ability of the solvent.[13] The correlation coefficient is $r^2 = 0.94$ for the Kamlet−Taft parameter α[24] and $r^2 = 0.92$ for the Catalán parameter SA[25] (see Table S1 and Figure S1 in the Supporting Information). Some confirmation of the enol−keto equilibrium changes in protic solvents was obtained by the PM6 calculations (see Table S2a,b, Supporting Information). The stabilization energy due to intermolecular hydrogen bonds with alcohol molecule for the cis-keto tautomer is nearly twice greater than that for the enol one and is greater for HFIP than for MeOH.

To get insight into the stoichiometry of the BSP:HFIP complex, we have performed stationary absorption measurements of BSP in MeOH:HFIP mixtures (Figure S2, Supporting Information). However, the results are not clear and indicate that both 1:1 complex and that involving more HFIP molecules (probably three) are responsible for the blue shift of the maximum of the BSP enol band (Figure S2b, Supporting Information) and the keto−enol equilibrium changes (Figure S2c, Supporting Information).

In stationary fluorescence of BSP in HFIP (Figure 1), the dominant emission originates from the S_1 state of cis-keto tautomer (with a characteristic large Stokes' shift with respect to the enol absorption band) and has a maximum at 545 nm (the same as for BSP in TFE). The emission spectrum profile is the same for the excitation of the enol (360 nm) or keto band (440 nm). The fluorescence lifetime was measured to be 37−40 ps after excitation at 400 nm (and found to be constant in the spectral range 520−600 nm), which is only slightly longer than in TFE (35 ps).[13]

On the basis of our previous report on stationary studies of BSP in acidic solvent TFA,[13] the BSP cation (probably BSP with a fully protonated imino group NH^+; see Scheme 1) has different absorption maxima (at 346 and 409 nm) and emission

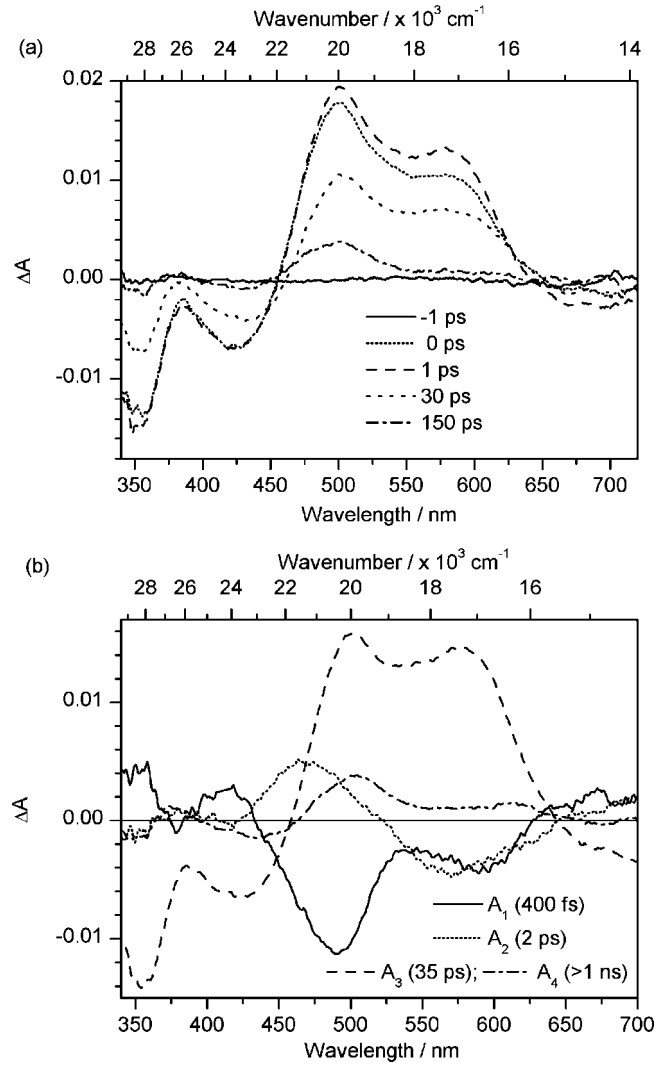

Figure 2. Transient absorption spectra of BSP in HFIP for selected time delays between the pump and probe pulses (a) and the wavelength-dependent amplitudes of the time constants (given in the inset) obtained by four-exponential global fit (b) presented in the linear scale of wavelength. The fwhm of the instrumental function used for convolution with the exponential functions was set as 150 fs.

spectrum (maximum at 484 nm). Therefore, the full protonation of BSP molecule does not take place in HFIP. The absorption of the reference system $BSPMe_2$ in TFA (Figure S3, Supporting Information) is nearly the same as that of BSP, which means that the BSP cation is generated in the enol tautomer in TFA. The lifetime of the BSP fluorescence in TFA was measured to be 25−30 ps in the spectral range 485−600 nm after excitation at 400 nm. The lifetime is thus similar to the duration of cis-keto emission in EtOH, in which the fluorescence quantum yield is about 5 times smaller.[13] It means that the radiative rate constant for the BSP enol cation is much higher than that for BSP anti-enol tautomer.

The femto- and picosecond transient absorption spectra of BSP in HFIP under excitation at 400 nm are presented in Figure 2a. According to our knowledge, the time-resolved studies of photochromic Schiff bases in this solvent have been reported here for the first time. The kinetic analysis of the transient absorption signals was performed in two ways: by fitting at single selected wavelengths (Figure 3) and in a global analysis approach (Figure 2b). The temporal broadening of the instrumental function due to the different group velocities of the pump and probe pulses in the sample can be nearly neglected in HFIP,

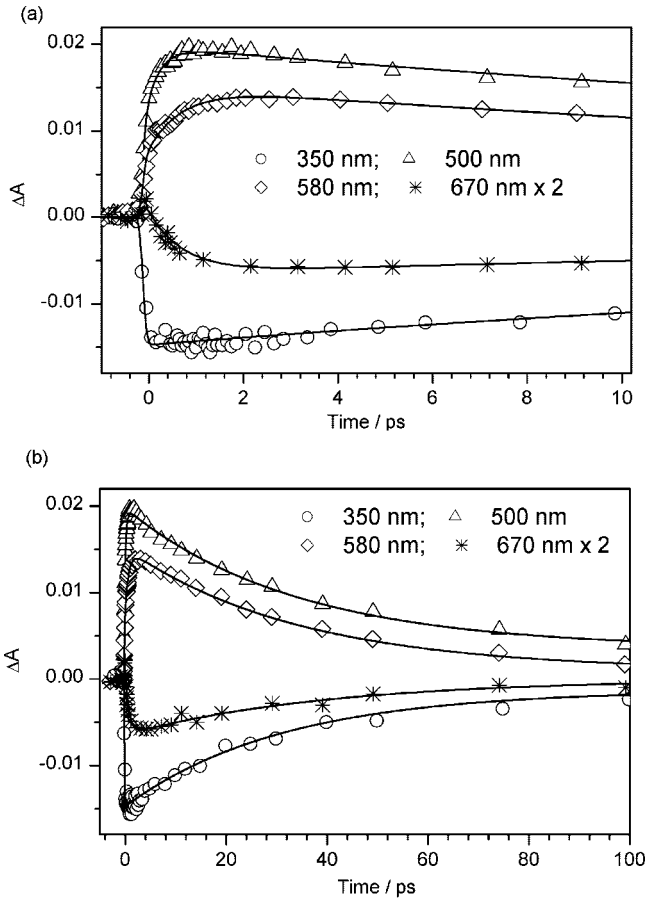

Figure 3. Examples of the kinetic curves of the transient absorption signals for BSP in HFIP, and the fits in shorter (a) and longer (b) time scale. The values of the fitted parameters [exponential functions $\Delta A(t) = A_1 \exp(-t/\tau_1) + A_2 \exp(-t/\tau_2) + A_0$ convoluted with the instrumental function of 150 fs fwhm] are the following: 350 nm, $A_1 = -0.0134$, $\tau_1 = 31$ ps, $A_0 = -0.0013$; 500 nm, $A_1 = -0.0063$, $\tau_1 = 290$ fs, $A_2 = 0.0161$, $\tau_2 = 34$ ps, $A_0 = 0.0036$; 580 nm, $A_1 = -0.0071$, $\tau_1 = 710$ fs, $A_2 = 0.0141$, $\tau_2 = 35$ ps, $A_0 = 0.0010$; 670 nm, $A_1 = 0.0037$, $\tau_1 = 740$ fs, $A_2 = -0.0032$, $\tau_2 = 40$ ps, $A_0 = 0$.

since the refractive index dispersion in this solvent is much smaller than in, for example, ACN and EtOH.[13,26] Therefore, the global analysis program[27] that calculates the convolution of the multiexponential functions with the constant instrumental function can be used (Figure 2a).

In contrast to the above-mentioned similarities of the results in HFIP to those in other alcohols, the femto- and picosecond transient absorption spectra show striking differences when compared to the results in TFE, EtOH, ACN, and HEX.[13] First, the negative ground-state depopulation band (below 450 nm) consists of two bands with maxima at 350 and 430 nm. The appearance of the new long-wavelength bleaching band in HFIP is the manifestation of the strong stationary absorption band of the cis-keto form. Second, besides the previously observed transient absorption band from S_1 cis-keto state peaking around 500 nm, a new positive band around 580 nm occurs. Because of that, the negative stimulated emission signals (due to the emission of the cis-keto state) become dominant at longer wavelengths (>630 nm) than previously (>580 nm). Finally, besides the instantaneous (instrument function limited, <50 fs) increase in intensities of all above-mentioned bands, there is another ultrafast risetime component (varying from 250 fs to 1 ps) in both the transient absorption and stimulated emission bands (see Figure 3a). It should be noted that the measurements of BSP in ACN were also performed on the same day (and

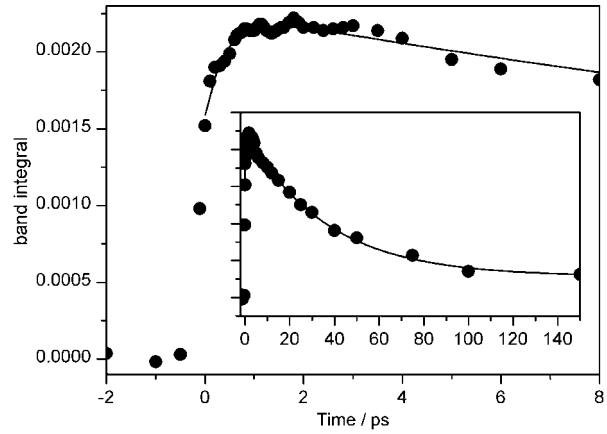

Figure 4. Band integral analysis of transient absorption signal (ΔA) of BSP in HFIP in shorter and longer time scale (inset). Band integral (BI) is calculated in the spectral range from $\lambda = 450$ to 700 nm as follows: $\mathrm{BI}(t) = \int(\Delta A(t,\lambda)/\lambda)\, d\lambda$.[28] The two-exponential fit gives the time constants of $\tau_1 = 415 \pm 35$ fs (risetime) and $\tau_2 = 35.2 \pm 1.4$ ps (decay time). Note that the no 2 ps component is present, which means it should be associated with the vibrational cooling process, in line with the global fitting analysis.

under the same experimental conditions) as those of BSP in HFIP and TFA, and the results were identical to those described previously[12] (in particular, no risetime components >50 fs in the transient absorption and stimulated emission signals were observed in ACN for wavelengths longer than 450 nm).

The global analysis revealed the sufficient quality of the fit when three-exponential functions were assumed with the following time components: 400 ± 150 fs, 2 ± 0.5 ps, and 35 ± 5 ps. The spectra of the amplitudes of the three time components (often referred to as the decay-associated spectra) are presented in Figure 2b. The 35 ps component manifested as the decay of all transient bands is in good agreement with the fluorescence lifetime of S_1 cis keto state. The residual transient absorption with a maximum at around 500 nm and a new (compared to weaker alcohols[13]) long-wavelength tail can be attributed to the long-lived photochromic transient (trans-keto tautomer). The interplay of two fastest components (400 fs and 2 ps) can rationalize the large spread of ultrafast rise times observed in two-exponential fittings at selected wavelengths (Figure 3).

The spectrum associated with the 400 fs component is similar to the initial transient absorption and stimulated emission signals, but has the opposite sign (Figure 2). Therefore, we assign it to the additional (slower) population channel of the initially (or within 50 fs) excited state (S_1 cis-keto state). On the other hand, the spectrum associated with the 2 ps component causes the rise of the transient absorption signal in the central part (from 500 to 650 nm) and the decay in the blue (<500 nm) and red (>650 nm) wings. Thus, it can reflect the narrowing of the transient absorption band, and we ascribe it to the vibrational cooling of the S_1 cis-keto state. Indeed, on the vibrational cooling process the area under the transient absorption band curve is constant.[28] The spectral integral of the amplitude of the 2 ps component (calculated as suggested in ref 28; see also Figure 4) is equal to 0 ± 5% of the spectral integral of the 35 ps component amplitude (in the limits 450−730 nm). On the contrary, the spectral integral of the 400 fs component amplitude is equal to 40 ± 10% and thus we connect it with the population dynamics.

It should be also emphasized that the true transient absorption spectrum of the S_1 state of the cis-keto tautomer is much

SCHEME 2: Schematic Representations of the Different Proton Transfer Processes in the BSP Molecule That Involve the Intermolecular Hydrogen Bonds[a]

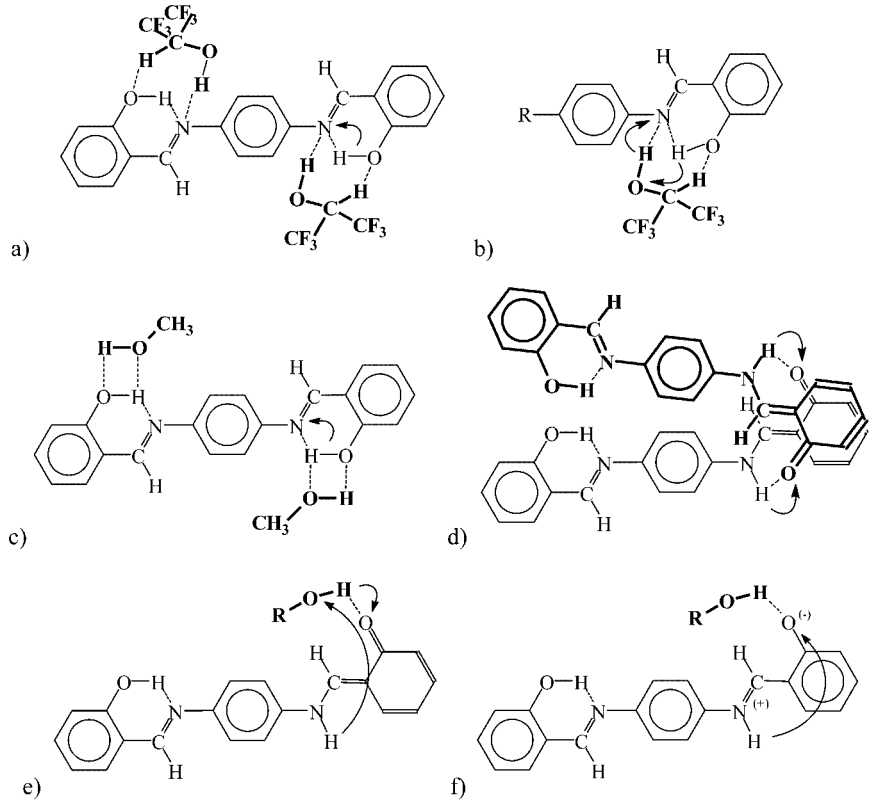

[a] For the details of the structures, see Table S2, Supporting Information.

different than that of the measured positive band because of the contribution from the stimulated emission. The true transient absorption spectrum can be estimated by subtracting from the experimental transient absorption data the fluorescence emission spectrum normalized to the negative signal at 700 nm (assuming that the contribution of the S_1 cis-keto state transient absorption can be neglected near 700 nm) (see Figure S4, Supporting Information). The obtained spectrum has one maximum around 550 nm and is significantly red-shifted with respect to the S_1 cis-keto spectra in HEX and EtOH obtained in an analogous way (Figure S4, Supporting Information).

The femto- and picosecond transient absorption of BSP in the acid confirm the conclusions drawn already from the stationary data, that in HFIP the BSP cation is not formed. Indeed, the transient spectra of BSP in TFA (Figure S5a, Supporting Information) are quite different from that in HFIP. After excitation at 400 nm, a positive transient absorption band with a maximum at about 590 nm appears, together with negative bleaching bands (matching stationary absorption profile) and the small negative band at 480 nm from the stimulated emission. The amplitudes of the bands decrease with the time constant of 30 ± 5 ps (in agreement with the fluorescence lifetime). Besides, a shorter time constant of 3.0 ± 0.5 ps is found in a global fit (Figure S5b, Supporting Information). The maximum amplitude of this component is red-shifted with respect to that of the longer component, and the 3.0 ps might be ascribed to the lifetime of the second conformer of enol cation (or the double protonated enol tautomer).

Next, we would like to discuss the origin of the 400 fs increase in the S_1 cis-keto state population observed for BSP in HFIP. If the pump pulse at 400 nm excites mainly the long-wavelength band (originating from the cis-keto tautomer), then the occurrence of the characteristic stimulated emission of S_1 cis-keto state for $\lambda > 630$ nm should be instantaneous. The delayed population of this state can be rationalized by the assumption that the pump pulse excites also another structure: a complex of BSP enol tautomer with HFIP molecule (or molecules) in which the excited-state proton transfer occurs. Such a solvent-assisted proton-transfer time constant (400 fs) for BSP in HFIP is ultrafast but longer than the previously measured (in HEX, ACN, EtOH, and TFE) intramolecular-proton-transfer time constant (<100 fs).[13] We may propose two explanations for this phenomenon: in the first one, the solvent molecule plays a passive role, while in the second one, the active role.

The first explanation is based on PM6 calculations of the complexes of BSP enol tautomer and alcohol molecule (Table S2a, Supporting Information, Scheme 2a,c). In the case of alcohols of hydrogen-bond-donating ability smaller than HFIP (like MeOH), the proton-accepting properties of their oxygen atom enable the formation of a double-hydrogen-bonded complex with the hydroxyl group of BSP (Scheme 2c and Table S2a, Supporting Information). Such a complex was also theoretically predicted for SA and MeOH,[29] and its formation does not weaken the intramolecular hydrogen bond (the distance between H and N atoms is the same as for the isolated enol tautomer and the energy of the hydrogen bond very well correlates with the inverse third power of the H-bond length[30]). In the case of HFIP, such a complex is not possible to form since the electron charge from the oxygen atom is strongly shifted toward fluorine atoms (zero value of β parameter of the Kamlet—Taft scale; see Table S1, Supporting Information). Instead, a new complex of HFIP with intermolecular hydrogen

bonds with both N and O atoms of BSP enol tautomer can be formed, since the hydrogen atom attached to the central carbon atom of HFIP is very protic (see Scheme 2a and Table S2a, Supporting Information). Such a complex might reduce the intramolecular proton transfer rate because (i) the intramolecular-hydrogen-bond length becomes longer (and thus weaker), (ii) the hydrogen atom of the BSP hydroxyl group is slightly out-of-plane, and (iii) the low-frequency vibrations modulating the O—N distance (which promote the ESIPT process) are altered by the bridging HFIP molecule.

To verify the reliability of the PM6 calculations for such complexes, we have also compared the results with the ab initio calculations for a simpler enol tautomer of SA (parent molecule to BSP) molecule. It revealed that, despite the PM6 method, the semiempirical results still underestimate the role of hydrogen bonds, since both the stabilization energies are higher and hydrogen-bonded distances are shorter in the structures optimized by the ab initio method (see Table S2d, Supporting Information). However, the main features of the complexes with MeOH and HFIP molecules are similar and the conclusions drawn previously are still valid.

Some confirmation of the new nature of complex of BSP with HFIP can be also found in the UV−vis and IR results obtained for SA and its derivatives in protic and acidic solvents.[31,32] The UV−vis absorption data indicate that, in the solvents with a proton-donating ability less than or equal to that of TFE, a single equilibrium exists for SA, whereas in the solvents with a proton-donating ability equal to or greater than that of HFIP, more than one equilibrium exist.[32] Moreover, new infrared bands appear in the spectra of SA in HFIP not observed in other solvents, and they are assigned to the $C{=}NH^+$ vibration from the protonated structure.[31,32] Our studies reveal that the BSP cation is not formed in HFIP. However, the strong proton-donating ability of that solvent might result in a proton shift from the solvent hydroxyl group to the BSP nitrogen greater than in a typical hydrogen-bonded complex, and thus, the vibration similar to $C{=}NH^+$ from the partially protonated nitrogen may occur.

The ability of HFIP to form a new (with respect to alcohols of lower hydrogen-bond-donation ability) complex with Schiff bases is also supported by the stationary measurements of $BSPMe_2$. The absorption maximum of this compound in all solvents is similar to that of the enol form of BSP, while the absorption of $BSPMe_2$ in HFIP shows a drastically new shape (Figure S6a, Supporting Information). Also, the fluorescence quantum yield in this solvent becomes 2 orders of magnitude higher than in the other solvents, for example, in TFE (Figure S6b, Supporting Information). These new features have to be due to the formation of complexes in the enol form since the keto structure formation is not possible for $BSPMe_2$.

All the above observations have led to the second explanation of the slowing down of the proton transfer rate to $(400\ \text{fs})^{-1}$. Taking into account the very strong proton-donating properties of HFIP, the intermolecular hydrogen bond with BSP nitrogen atom can be stronger than the intramolecular one and, therefore, instead of the intramolecular proton transfer, a double proton transfer via the solvent bridge can occur after the excitation—from HFIP oxygen to BSP nitrogen and from BSP oxygen to HFIP oxygen—like in Scheme 2b. The theoretical calculations do not directly confirm this assumption, since the intramolecular hydrogen bond in the enol tautomer is always shorter than the intermolecular one (see Table S2, Supporting Information). However, the most reliable ab initio calculations for SA predict the intermolecular hydrogen-bond length (2.00 Å) to be not much longer than the intramolecular one (1.85 Å). Taking into account the correlation between the H-bond length and its energy,[30] the intermolecular bond has only 20% smaller energy than the intramolecular one. Moreover, the involvement of more than one HFIP molecule in the complex might increase the acidity of the alcohol's hydrogen due to the cooperative effect between hydrogen bonds[33] and make the intermolecular hydrogen bond even shorter. Such cationlike species, distinguishable from both the typical hydrogen-bonded complexes and the cations with fully protonated nitrogen, have been reported in HFIP.[33] The optimization involving more alcohol's molecules has not been calculated.

The mechanism of the solvent-assisted proton transfer via the solvent bridge consisting of one or more solvent molecules is similar in nature to the ESIPT.[34−36] The electron configuration change in the excited state (increased acidity in the proton-donor part and basicity in the proton-acceptor part) provides the driving force for the proton transfer reaction.[35] The cooperative low-frequency vibrations in the hydrogen-bonded solute−solvent complex shorten the distance between the proton-donor and proton-acceptor parts and play the active role in the proton transfer.[34,36]

Usually, the time constant of the solvent-mediated excited-state proton transfer is reported to be much longer than hundreds of femtoseconds.[37,38] In most cases, the rearrangement of solvent molecules after excitation is necessary, which slows down its overall dynamics.[39] A fast process in excited-state requires that the proton transfer takes place along the intermolecular hydrogen bonds that exist already in the ground-state complex. There are few reports on subpicoseconds time scale of such proton transfer. For example, in hydrogen-bonded acid−base complexes, the proton transfer proceeds within 150 fs,[40] and intermolecular double proton transfer within a "cyclic" solute−solvent complex of carbazole-related compounds in alcohols takes place with a time constant of 600−900 fs (the faster component).[39]

Therefore, to conclude, we are not able to choose definitely between the two proposed mechanisms (Scheme 2, parts a and b) of ultrafast proton transfer observed for BSP in HFIP. It should be noted that both mechanisms cannot be treated as rigorous interpretation of the possible process. The proton transfer reaction is governed by a multidimensional potential energy surface that is very complicated for hydrogen-bonded complexes. Even for typical solvated clusters in the gas phase like 7-hydroxyquinoline with three ammonia molecules[41] or 7-azaindole with two methanol molecules,[34] the process of solvent-assisted proton transfer has not been well understood. At present, the system studied in this work is too complicated to obtain excited-state potential energy surface with reliable calculation methods.

BSP Photochrome Lifetimes in Differently Interacting Solvents. The nano- and microsecond transient absorption permits a study of the lifetime of the photochromic transient (trans-keto tautomer) of BSP in solution at room temperature. So far the results of transient absorption only in ACN have been reported for this compound[4,5] and the lifetime of the ground-state of the trans-keto photochrome (about 3 ms) was deduced from the decay of the positive signal in the visible spectral range (400−600 nm). Thus, we decided to extend the studies to a number of other different solvents (HEX, EtOH, MeOH, TFE, HFIP and TFA) as well as to the ultraviolet spectral region (300−400 nm) where the changes in the negative ground-state depopulation signal occur.

The selected transient absorption data are shown in Figure 5. The spectra profiles were constructed from the one- or two-

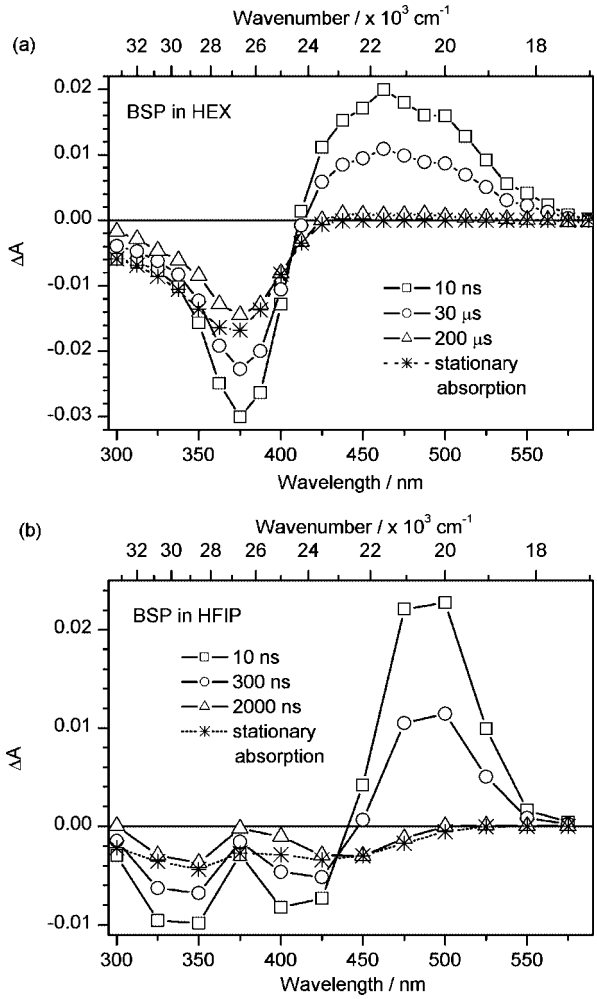

Figure 5. Transient absorption of BSP in HEX (a) and HFIP (b) on nano- and microsecond time scale presented in the linear scale of wavelength. The stationary absorption spectra normalized to the measured final depopulation bands are also shown.

TABLE 1: Photochrome Lifetime of BSP in Selected Solvents, Calculated as a Result of One-Exponential (τ) or Two-Exponential (τ_1 and τ_2) Global Fit in the Spectral Range 300−600 nm, $c \sim 3 \times 10^{-5}$ M

solvent	τ (μs)	τ_1 (μs)	τ_2 (μs)
HEX	50	20 (decay, 60%)	100 (decay, 40%)
ACN[a]	700	600 (decay, 100%)	100 (rise, 10%)
EtOH	300	250 (decay, 100%)	130 (rise, 30%)
MeOH	150	–	–
TFE	15	–	–
HFIP	0.45	–	–

[a] The time constants in ACN might be uncertain, due to the limited temporal range of measurements (500 μs).

exponential functions fitted to the kinetics recorded at particular wavelengths. Similarly as for the femtosecond transient absorption data, the global analysis was also used to verify the time constants obtained (see Figures S7 and S8, Supporting Information). Table 1 summarizes the fitted time constants in different solvents. We found no effect of oxygen (checked for ACN and TFA), which means that the transient absorption from the triplet state does not contribute to the measured signals, and thus, the time constants can be safely assigned to the lifetime of photochromic transient. In ACN, EtOH, and HEX, the fit is much improved when two-exponential decays are assumed (see also Figure S7, Supporting Information). Two time components in ACN and EtOH might suggest the presence of another conformer of the trans-keto tautomer, which is not surprising taking into account the flexibility of the BSP structure. The spectrum of the amplitudes of the second time component is different from the amplitude spectrum of the main one, and the former have the opposite sign (risetime) to that of the latter (decay time). Therefore, in ACN and EtOH the second conformer probably populates the main conformer. In HEX, the amplitudes of both components have very similar spectra (see Figure S7b, Supporting Information), which probably reflects the nonexponential decay of the single species and is discussed below.

Three characteristic features of the BSP photochrome lifetime, reported sometimes for SA or its derivatives, should be pointed out.[15,22,42,43] First, the lifetime significantly increases when going from nonpolar HEX to polar ACN. This suggests that the barrier for the re-enolization is higher in the polar environment and the ground-state of the photochrome is greater stabilized in ACN due to a significant dipole moment.

Second, we have checked the concentration dependence of the decay of the signal from the photochrome in HEX and found that the lifetime increases (for constant pump intensity) in less concentrated solutions (Figures 6 and S9, Supporting Information). This can be rationalized by the deactivation process that involves the complex of two BSP molecules, and similarly as for comparable systems,[42,44,45] the second-order double proton transfer re-enolization can be proposed (see Scheme 2d). As mentioned earlier, the photochromic decay in HEX cannot be fitted by the single-exponential function (as for a first-order process). The kinetics of the decay is also not well reproduced by the pure second-order reaction (reciprocal function). However, we have successfully fitted it to the mixed first- and second-order case, where the normalized kinetics can be expressed as follows:[46]

$$\Delta A(t) = \frac{1 - m}{e^{k_1 t} - m} \qquad (1)$$

where $m = 2c_P k_2/(k_1 + 2c_P k_2)$ is the shape parameter ($m = 1$ for pure second-order reaction and $m = 0$ for pure first-order reaction), k_1 is the first-order rate constant (intramolecular back trans−cis isomerization around the C=C(phenyl) bond), k_2 is the second-order rate constant, and c_P is the concentration of the photochrome tautomer. As expected, the fitted k_1 values are nearly constant for all BSP concentrations, while the $c_P k_2$ values increases proportionally to the BSP concentrations (see Figure 6b and the figure caption), which supports the proposed model. Only for very dilute solutions does the first-order process dominate over the second-order double proton transfer. The concentration dependence probably also explains the different photochrome lifetimes of Schiff bases reported in the literature, in particular the discrepancy between our result of BSP in ACN (about 700 μs) and that in refs 4, 5 (3 ms).

Further evidence for the complex structure presented in Scheme 2d has been also provided by the linear dependence of the second-order rate on the intensity of the pump pulse, in line with similar systems.[44,45] As can be seen in Figure 6b, the $c_P k_2$ values depend linearly not only on the BSP concentration but are also linearly proportional to the pump pulse intensity, which implies that the deactivation rate depends not on the concentration of the initial enol form but on the concentration of the species created after excitation. This supports the bimolecular double proton transfer in the complex of two photochrome

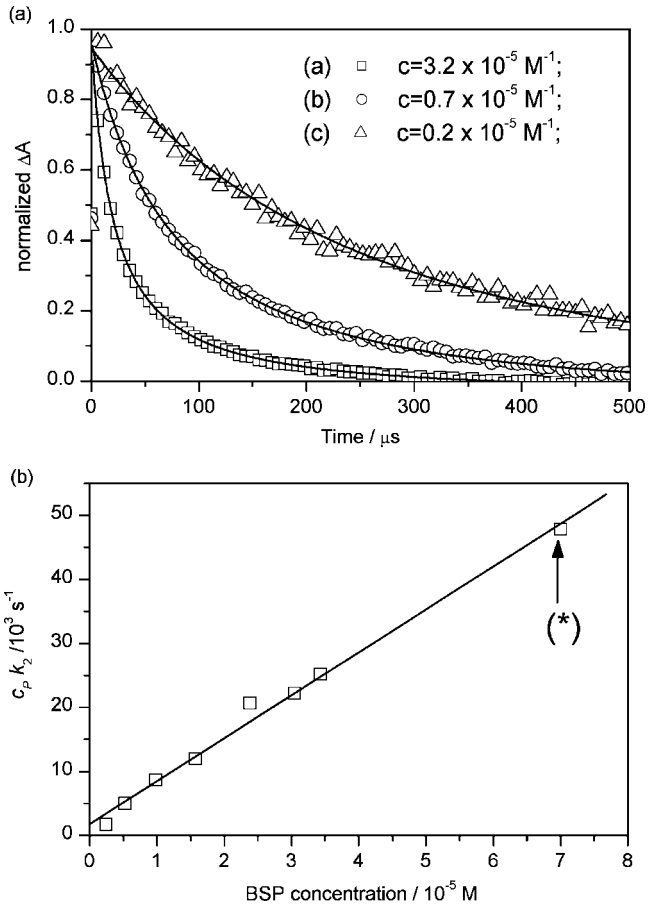

Figure 6. (a) Normalized kinetic curves of the transient absorption signals of BSP in HEX (462 nm) on a microsecond time scale for different BSP concentration c with the fitted function according to eq 1. For clarity, the experimental data are smoothed and only every 150th experimental point is shown. The fitted parameters are (a) for $c = 3.2 \times 10^{-5}$ M, $k_1 = 2.9 \times 10^3$ s^{-1} and $m = 0.94$ (thus $c_P k_2 = 22.7 \times 10^3$ s^{-1}); (b) for $c = 0.7 \times 10^{-5}$ M, $k_1 = 4.0 \times 10^3$ s^{-1} and $m = 0.72$ (thus $c_P k_2 = 5.2 \times 10^3$ s^{-1}); and (c) for $c = 0.2 \times 10^{-5}$ M, $k_1 = 3.2 \times 10^3$ s^{-1} and $m = 0.30$ (thus $c_P k_2 = 0.7 \times 10^3$ s^{-1}). (b) Dependence of $c_P k$ values on the BSP concentration in HEX (squares) together with the linear fit (solid line). The last point denoted with an asterisk was obtained not by an increase in BSP concentration (3.1×10^{-5} M) but by a 2.3 increase in the pump pulse intensity.

molecules as the process responsible for the photochrome deactivation.

The PM6 calculations also support the formation of BSP trans-keto dimer with two intermolecular hydrogen bonds with the stabilization of about 12 kcal/mol (see Table S2c, Supporting Information). The deformation from planarity of both molecules should enable the cooperative motion of the hydrogen-bonded network and the proton transfer due to out-of-plane vibrations. Of course, the time scale of this process might be several orders of magnitude longer than the ultrafast excited-state proton transfers discussed in previous sections, and it is not possible to distinguish whether it is a concerted or sequential process.

These data indicate that the decay of the photochromic transient and the return to the initial enol form nearly do not take place through the ground-state of the cis-keto tautomer, which is in contrast to the commonly assumed deactivation schemes for aromatic Schiff bases (see Schemes 3 and S1, Supporting Information). The possibility of rotation around the double C=C(phenyl) bond (back trans−cis isomerization) is strongly suppressed in the ground state. Instead, the photochrome deactivation takes place via the re-enolization in the

SCHEME 3: Proposed Deactivation Scheme of BSP

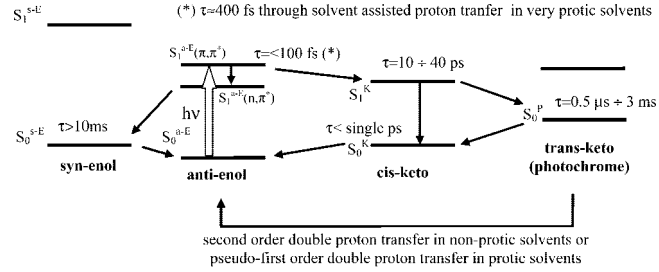

trans structure and, after that the rotation around the single C−C(phenyl) bond, easily leads to the initial closed enol form (with intramolecular hydrogen bond).

Third, the energy barrier for the re-enolization decreases in more protic solvents (3 orders of magnitude from ACN to HFIP). Indeed, there is quite a good linear correlation between the log(k_{reenol}) value (the re-enolization rate constant k_{reenol} is defined as the reciprocity of the photochrome lifetime) and the hydrogen bond donation ability parameter α (Figure S10, Supporting Information). For BSP in MeOH, TFE, and HFIP, a monoexponential decay was observed, which indicates a purely first-order deactivation process. This effect might be explained by the solvent-assisted re-enolization involving the intermolecular proton exchange in the complex of BSP with solvent molecule (or molecules).[42,47]

In order to get insight into the stechiometry of such a complex, a series of measurements with varying concentration of different alcohols added to nonpolar and polar solvents was performed. The decay of the photochrome was analyzed by fitting the kinetics measured at 450 or 475 nm with eq 1, and the concentration dependence of the (pseudo-)first-order rate constant k_1 was investigated (in this case, k_1 represents the rate of intermolecular proton exchange). The most pronounced effect was observed when HFIP was added to BSP solution in HEX (see Figure 7a). The slope of the linear function fitted to the data in the log−log scale represents the number of alcohol molecules that make the complex with BSP,[47] and the fitted value close to 1 indicates that the catalysis of the BSP photochrome lifetime takes place in the complex between one photochrome and one solvent molecule. As can be seen in the inset in Figure 7a, the participation of the second-order photochrome deactivation (in the BSP dimer) gradually decreases with increasing concentration of HFIP (from the m values close to 1 to the values close to 0).

In all other cases, a linear dependence of k_1 on the alcohol concentration was also observed (Figure 7b and Figure S11, Supporting Information). Interestingly, for alcohols in nonpolar solvent, the rate of the photochrome decay increases up to a concentration of about 0.1 M (where the rate is higher than in bulk alcohol) and then gradually decreases to the value in pure alcohol (Figure S11, Supporting Information). This result can be rationalized by the effect of polarity on the photochrome lifetime. For low alcohol concentrations, the specific interactions take place in the nonpolar environment, but when the concentration is high enough, the alcohol molecules induce the increase in polarity around the BSP molecule, which increases the photochrome lifetime (see a comparison between HEX and ACN discussed above). Table 2 presents the rate of the photochrome deactivation catalysis for different alcohols in different environments. As can be seen, the rate for the most protic HFIP in nonpolar solvent (HEX) is about an order of magnitude higher than that for TFE and two orders higher than that for MeOH. On the other hand, for the same alcohol the rate of catalysis is

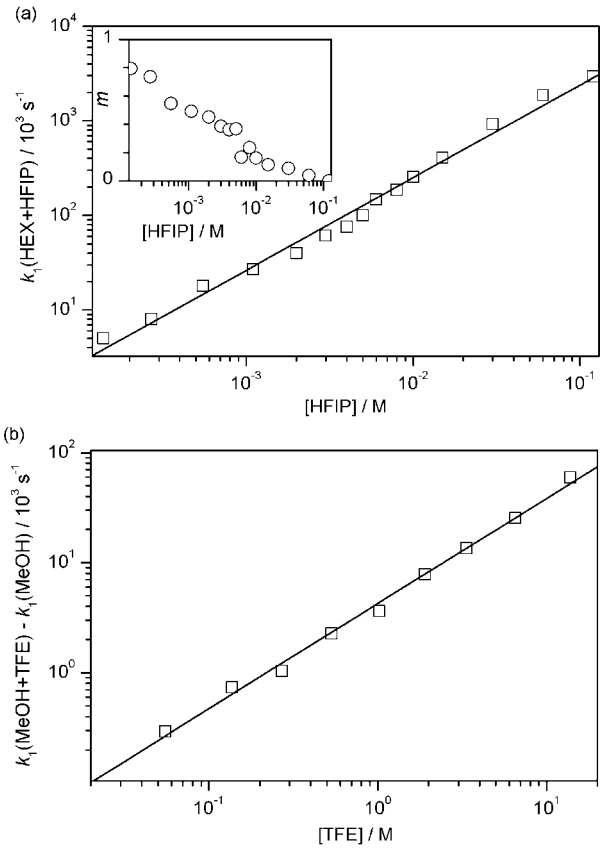

Figure 7. First order rate constant k_1 (squares, obtained from eq 1, fitted to the decay of transient absorption signal of photochrome at 475 nm) for varying concentrations of HFIP in BSP solution in HEX (a) and TFE in BSP solution in MeOH (b). The solid line represents the linear fit with the following parameters: (a) slope 0.98 ± 0.03, intercept 4.36 ± 0.07 and (b) slope 0.96 ± 0.02, intercept 0.63 ± 0.02. The inset in part a shows the dependence of the parameter m (from eq 1) on the concentration of HFIP.

TABLE 2: Rate of the BSP Photochrome Deactivation Catalysis for Different Alcohols in Different Environments

alcohol in environment	rate of photochrome deactivation catalysis/s^{-1} M^{-1}
HFIP in *n*-HEX	2.6×10^7
TFE in *n*-HEX	1.9×10^6
MeOH in *n*-HEX	1.1×10^5
TFE in MeOH	4.3×10^3
MeOH in ACN	1.6×10^2

largely decreased (about 3 orders of magnitude) in polar solvents (MeOH and ACN) compared to nonpolar ones.

The 1:1 stoichiometry of the BSP−alcohol complex can be compared to the results obtained for a similar but more rigid system, 2-(2′-hydroxyphenyl)-3*H*-indole (HBC).[47] In those studies, the 1:2 complex was observed when adding EtOH or MeOH to HBC in 3-methylpentane solution and the re-enolization was explained by the triple proton transfer via the solvent bridge formed by two alcohol molecules. For BSP, the participation of fewer alcohol molecules than for HBC (one instead of two) makes it impossible to form the solvent bridge between the nitrogen and oxygen atoms in the photochrome structure, as was also confirmed by PM6 optimization (Table S2c, Supporting Information). Therefore, two other rationalizations can be proposed. If the back proton transfer in the BSP molecule takes place through the intermolecular exchange of the hydrogen atom (as schematically presented in Scheme 2e), than it must consist of two separated processes: hydrogen abruption from the alcohol hydroxyl group by the oxygen atom of the BSP keto group and than the attachment of the hydrogen atom from nitrogen to the so-formed anion. Another possibility is that the intermolecular hydrogen bond with alcohols induce the shift of electron density toward the oxygen atom of the BSP keto group, which decreases the double bond character of the C═C(phenyl) bond (see Scheme 2f). As a result, the probability of rotation around this bond and back trans−cis isomerization drastically increase. In this case, the proton transfer would be intramolecular with the more passive role of alcohol.

Another important thing is that the intensity of the depopulation band decreases by only about 60−80% within the decay of the photochrome tautomer in all solvents and after that the residual negative transient absorption signal stays constant up to 500 μs (the temporal range of the measurements) (see Figures 5 and S7 and S8, Supporting Information). We also performed the nanosecond transient absorption experiment for $BSPMe_2$ in ACN and found for this compound only the constant negative depopulation band (Figure S12, Supporting Information). Since for $BSPMe_2$ the photochromic cycle is not involved in the deactivation, the transient species that is responsible for the very long-living trap should be connected with the enol form. Therefore, similarly as for the hydroquinone family of Schiff bases recently studied by us[15] and in line with the previous assumptions for other Schiff bases,[22,43,48] we assign this long-lived transient to the ground-state of the syn-enol tautomer of BSP (see Schemes 1 and 3). Probably, the ground-state absorption of this tautomer is blue-shifted with respect to that of the initial antienol form, as was observed for a similar benzylidenoaniline molecule.[49] It explains why the transient absorption signal in the shorter wavelength range has less negative intensity than that expected when the stationary absorption spectrum is normalized to the depopulation band measured (Figures 5 and S13, Supporting Information); in that spectral region, a positive transient absorption from the ground-state of the syn-enol tautomer must contribute. The anti-syn isomerization can quickly take place in the excited state, but in the ground state, the backward rotation around the C═N double bond might be very slow; thus, the lifetime of the syn-enol tautomer is even longer than for that of the photochromic trans-keto tautomer.

As mentioned in the Introduction, our recent studies of BSP have revealed that there is an efficient deactivation channel within the enol form—the electronic relaxation to the $S_1(n,\pi^*)$ anti-enol state—competing with the ESIPT and photochromic cycle.[13] Similar conclusions have been recently drawn from the resonance-enhanced multiphoton ionization measurements of SA.[50] Also, the calculations for the SA molecule and its derivatives predict the existence of the $S_1(n,\pi^*)$ anti-enol state with the perpendicular geometry of two phenyl rings, which has slightly lower energy than the planar $S_1(\pi,\pi^*)$ anti-enol state.[51] The perpendicular position of the phenyl rings in the $S_1(n,\pi^*)$ anti-enol state may favor the anti-syn isomerization around the C═N bond, since the transition state of similar geometry has been suggested for such isomerization in similar benzylideneaniline.[49,52] Therefore, we propose that this deactivation might at least partially lead to the syn-enol form and the $S_1(n,\pi^*)$ anti-enol state might be a precursor of the ground state of the BSP syn-enol tautomer (see Schemes 3 and S1, Supporting Information). Like in the findings from the previous paragraph, it should be pointed out that the occurrence of

additional tautomer (syn-enol) is in contrast to the commonly assumed photochromic cycle of Schiff bases from the family of SA.

In all solvents studied, the maximum of the trans-keto photochrome absorption is similar and located between 450 and 500 nm. Its spectral shape matches the residual transient absorption observed in femto- and picosecond transient absorption.[12,13] The only difference is found in HFIP, for which no long-wavelength band near 600 nm is observed in the nanosecond time scale. The probable explanation of that is the different excitation wavelength in both experiments (355 and 400 nm), since the excitation at 400 nm might populate another conformer of the BSP photochrome, most likely the previously discussed complex with strong intermolecular hydrogen bonds to the HFIP molecules.

Finally, we have also measured the nano- and microsecond transient absorption for BSP in TFA (see Figure S13, Supporting Information). The results in the acid also seem to be quite different for the excitation at 355 and 400 nm. The dominant signal in the microsecond time scale is the negative depopulation band (with two maxima corresponding to the stationary absorption profile) after the excitation at 355 nm, whereas the residual transient absorption signal in the picosecond time scale forms a positive band centered around 450 nm after excitation at 400 nm (Figure S4, Supporting Information). However, the decay of this band, proceeding with the time constant of about 6 μs, can be also recognized as the small changes superimposed on the depopulation band (Figure S13, Supporting Information). In analogy to other solvents, the long-standing depopulation band might indicate the presence of anti-syn isomerization of the BSP cation, which is more efficient for shorter wavelength excitation. While the unambiguous association of the long-lived transients to the exact tautomers of the BSP cation is rather uncertain, their existence definitely indicates that the conformational changes take place in this protonated molecule and they participate (at least partially) in a relatively fast decay of the cation fluorescence.

Conclusions

The most important findings from this paper concerning the BSP molecules (probably also relevant for many other Schiff bases) are the following (and are summarized also in Scheme 3):

(1) The evidence of formation of a new hydrogen-bonded complex of BSP with a very strongly proton-donating solvent molecule (HFIP) is provided. This complex is different from both the hydrogen-bonded complex of BSP with "typical" alcohols and the BSP cation formed in the acid.

(2) The solvent-assisted excited-state proton transfer takes place in the time scale of about 400 fs in HFIP.

(3) The photochromic transient deactivates in solution by means of three processes, and two of them involve intermolecular hydrogen bonds. In nonprotic solvents, double proton transfer in the complex of two BSP molecules takes place. In a protic environment, the photochromic decay is catalyzed in the complex between one BSP molecule and one solvent molecule. The lifetime of the photochromic transient varies by nearly 4 orders of magnitude for different solvents and concentrations.

(4) The creation of the ground-state of the syn-enol isomer is a result of the deactivation within the enol form that efficiently competes with the photochromic cycle in solution. The lifetime of the syn-enol isomer is even longer than that of the photochrome.

Acknowledgment. This work was performed under financial support of the Ministry of Science and Higher Education (MNiSW) Poland, project N204 149 32/3777. Dynamic measurements were made in the Center for Ultrafast Laser Spectroscopy at the A. Mickiewicz University in Poznan, Poland. Prof. Andrzej Maciejewski is kindly acknowledged for fruitful discussion during the work and reading the manuscript, and Prof. Jacek Koput is thanked for making the ab initio calculations. The authors also thank Dr. Krzysztof Dobek and Dr. Dariusz Komar for permission to use their fitting program for time-resolved emission data and Mrs. Katarzyna Filipczak and Mrs. Julia Józkowiak for technical support.

Supporting Information Available: Tables S1 and S2, Figures S1−S13, and Scheme S1. This material is available free of charge via the Internet at http://pubs.acs.org.

References and Notes

(1) Irie, M. *Chem. Rev.* **2000**, *100*, 1683.
(2) Andes, R. V.; Manikowski, D. M. *Appl. Opt.* **1968**, *7*, 1179.
(3) Sliwa, M.; Letard, S.; Malfant, I.; Nierlich, M.; Lacroix, P. G.; Asahi, T.; Masuhara, H.; Yu, P.; Nakatani, K. *Chem. Mater.* **2005**, *17*, 4727.
(4) Kownacki, K.; Kaczmarek, Ł.; Grabowska, A. *Chem. Phys. Lett.* **1993**, *210*, 373.
(5) Kownacki, K.; Mordzinski, A.; Wilbrandt, R.; Grabowska, A. *Chem. Phys. Lett.* **1994**, *227*, 270.
(6) Rosenfeld, T.; Ottolenghi, M.; Meyer, A. Y. *Mol. Photochem.* **1973**, *5*, 39.
(7) Knyazhansky, M. I.; Metelitsa, A. V.; Kletskii, M. E.; Millov, A. A.; Besugliy, S. O. *J. Mol. Struct.* **2000**, *526*, 65.
(8) Hoshino, N.; Inabe, T.; Mitani, T.; Maruyama, Y. *Bull. Chem. Soc. Jpn.* **1988**, *61*, 4207.
(9) Ito, E.; Oji, H.; Araki, T.; Oichi, K.; Ishii, H.; Ouchi, Y.; Ohta, T.; Kosugi, N.; Maruyama, Y.; Naito, T.; Inabe, T.; Seki, K. *J. Am. Chem. Soc.* **1997**, *119*, 6336.
(10) Li, S. Y.; He, L. M.; Xiong, F.; Li, Y.; Yang, G. Q. *J. Phys. Chem. B* **2004**, *108*, 10887.
(11) Zhang, Y.; Lu, Z. H. *Mater. Chem. Phys.* **1999**, *57*, 253.
(12) Ziółek, M.; Kubicki, J.; Maciejewski, A.; Naskręcki, R.; Grabowska, A. *Chem. Phys. Lett.* **2003**, *369*, 80.
(13) Ziółek, M.; Kubicki, J.; Maciejewski, A.; Naskręcki, R.; Grabowska, A. *J. Chem. Phys.* **2006**, *124*, 124518.
(14) Ziółek, M.; Kubicki, J.; Maciejewski, A.; Naskręcki, R.; Grabowska, A. *Phys. Chem. Chem. Phys.* **2004**, *6*, 4682.
(15) Ziółek, M.; Burdziński, G.; Filipczak, K.; Karolczak, J.; Maciejewski, A. *Phys. Chem. Chem. Phys.* **2008**, *10*, 1304.
(16) Wróżowa, T.; Ciesielska, B.; Komar, D.; Karolczak, J.; Maciejewski, A.; Kubicki, J. *Rev. Sci. Instrum.* **2004**, *75*, 3107.
(17) Maciejewski, A.; Naskręcki, R.; Lorenc, M.; Ziółek, M.; Karolczak, J.; Kubicki, J.; Matysiak, M.; Szymański, M. *J. Mol. Struct.* **2000**, *555*, 1.
(18) Burdziński, G.; Maciejewski, A.; Buntinx, G.; Poizat, O.; Lefumeux, C. *Chem. Phys. Lett.* **2004**, *384*, 332.
(19) Stewart, J. J. P. *J. Mol. Model.* **2007**, *13*, 1173.
(20) Stewart, J. J. P. *MOPAC2007*; Stewart Computational Chemistry: Colorado Springs, CO, 2007; http://OpenMOPAC.net.
(21) Frisch, M. J.; Trucks, G. W.; Schlegel, H. B.; Scuseria, G. E.; Robb, M. A.; Cheeseman, J. R.; Montgomery, J., J. A.; Vreven, T.; Kudin, K. N.; Burant, J. C.; Millam, J. M.; Iyengar, S. S.; Tomasi, J.; Barone, V.; Mennucci, B.; Cossi, M.; Scalmani, G.; Rega, N.; Petersson, G. A.; Nakatsuji, H.; Hada, M.; Ehara, M.; Toyota, K.; Fukuda, R.; Hasegawa, J.; Ishida, M.; Nakajima, T.; Honda, Y.; Kitao, O.; Nakai, H.; Klene, M.; Li, X.; Knox, J. E.; Hratchian, H. P.; Cross, J. B.; Bakken, V.; Adamo, C.; Jaramillo, J.; Gomperts, R.; Stratmann, R. E.; Yazyev, O.; Austin, A. J.; Cammi, R.; Pomelli, C.; Ochterski, J. W.; Ayala, P. Y.; Morokuma, K.; Voth, G. A.; Salvador, P.; Dannenberg, J. J.; Zakrzewski, V. G.; Dapprich, S.; Daniels, A. D.; Strain, M. C.; Farkas, O.; Malick, D. K.; Rabuck, A. D.; Raghavachari, K.; Foresman, J. B.; Ortiz, J. V.; Cui, Q.; Baboul, A. G.; Clifford, S.; Cioslowski, J.; Stefanov, B. B.; Liu, G.; Liashenko, A.; Piskorz, P.; Komaromi, I.; Martin, R. L.; Fox, D. J.; Keith, T.; Al-Laham, M. A.; Peng, C. Y.; Nanayakkara, A.; Challacombe, M.; Gill, P. M. W.; Johnson, B.; Chen, W.; Wong, M. W.; Gonzalez, C.; Pople, J. A. *Gaussian 03, Revision C.02*; Gaussian, Inc.: Wallingford, CT, 2004.
(22) Ohshima, A.; Momotake, A.; Arai, T. *J. Photochem. Photobiol. A: Chem* **2004**, *162*, 473.
(23) Turbeville, W.; Dutta, P. K. *J. Phys. Chem.* **1990**, *94*, 4060.
(24) Taft, R. W.; Kamlet, M. J. *J. Am. Chem. Soc.* **1976**, *98*, 2886.

(25) Catalán, J. Solvent effects based on pure solvent scales. In *Handbook of Solvents*; Wypych, G., Ed.; ChemTec Publishing: Toronto, Canada, 2001; pp 583.

(26) Schwan, C.; Penzkofer, A.; Marx, N. J.; Drexhage, K. H. *Appl. Phys. B: Laser Opt.* **1993**, *57*, 203.

(27) Katilius, E.; Hindorff, J.; Woodbury, N. ASUFIT program available at www.public.asu.edu/∼laserweb/asufit/asufit.html.

(28) Kovalenko, S. A.; Schanz, R.; Farztdinov, V. M.; Henning, H.; Ernsting, N. P. *Chem. Phys. Lett.* **2000**, *323*, 312.

(29) Vargas, V.; Amigo, L. *J. Chem. Soc. Perkin Trans. 2* **2001**, 1124.

(30) Rozenberg, M.; Loewenschuss, A.; Marcus, Y. *Phys. Chem. Chem. Phys.* **2000**, *2*, 2699.

(31) Ledbetter, J. J. W. *J. Phys. Chem.* **1977**, *81*, 54.

(32) Lewis, J. W.; Sandorfy, C. *Can. J. Chem.* **1982**, *60*, 1727.

(33) Carmona, C.; Balón, M.; Galán, M.; Angulo, G.; Guardado, P.; Muñoz, M. A. *J. Phys. Chem. A* **2001**, *105*, 10334.

(34) Sakota, K.; Komoto, Y.; Nakagaki, M.; Ishikawa, W.; Sekiya, H. *Chem. Phys. Lett.* **2007**, *435*, 1.

(35) Kyrychenko, A.; Waluk, J. *J. Phys. Chem. A* **2006**, *110*, 11958.

(36) Fernández-Ramos, A.; Smedarchina, Z.; Zgierski, Z. *J. Chem. Phys.* **2000**, *113*, 2662.

(37) Kwon, O.-H.; Jang, D.-J. *J. Phys. Chem. B* **2005**, *109*, 20479.

(38) Mehata, M. S. *J. Phys. Chem. B* **2008**, *112*, 8383.

(39) Marks, D.; Zhang, H.; Borowicz, P.; Waluk, J.; Glasbeek, M. *J. Phys. Chem. A* **2000**, *104*, 7167.

(40) Rini, M.; Magnes, B.-Z.; Pines, E.; Nibbering, E. T. J. *Science* **2003**, *301*, 349.

(41) Tanner, C.; Manca, C.; Leutwyler, S. *Science* **2003**, *302*, 1736.

(42) Stephan, J. S.; Mordziński, A.; Ríos Rodríguez, C.; Grellmann, K. H. *Chem. Phys. Lett.* **1994**, *229*, 541.

(43) Ohshima, A.; Momotake, A.; Arai, T. *Bull. Chem. Soc. Jpn.* **2006**, *79*, 305.

(44) Al-Soufi, W.; Grellmann, K. H.; Nickel, B. *Chem. Phys. Lett.* **1990**, *174*, 609.

(45) Chou, P.-T.; Martinez, M. L.; Studer, S. L. *Chem. Phys. Lett.* **1992**, *195*, 586.

(46) Lavabre, D.; Pimienta, V.; Levy, G.; Micheau, J. C. *J. Phys. Chem.* **1993**, *97*, 5321.

(47) Stephan, J. S.; Ríos Rodríguez, C.; Grellmann, K. H.; Zachariasse, K. A. *Chem. Phys.* **1994**, *186*, 435.

(48) Becker, R. S.; Lenoble, C.; Zein, A. *J. Phys. Chem.* **1987**, *91*, 3509.

(49) Kobayashi, M.; Yoshida, M.; Minato, H. *Chem. Lett.* **1976**, 185.

(50) Okabe, C.; Nakabayashi, T.; Inokuchi, Y.; Nishi, N.; Sekiya, H. *J. Chem. Phys.* **2004**, *121*, 9436.

(51) Zgierski, M. Z.; Grabowska, A. *J. Chem. Phys.* **2000**, *112*, 6329.

(52) Ammal, S. C.; Yamataka, H. *Eur. J. Org. Chem.* **2006**, 4327.

JP803850N